Key Points:
- The dimension and structure of a hydrological models' active subspace are temporal scale-dependent
- Hydrological processes that are dominant on different temporal scales can be derived from the active subspace structure
- Methodology provides information on temporal scale-dependent parameter sensitivities

Correspondence to:
G. Chiogna,
gabriele.chiogna@tum.de

Temporal Scale-Dependent Sensitivity Analysis for Hydrological Model Parameters Using the Discrete Wavelet Transform and Active Subspaces

Daniel Bittner[1,2] , **Michael Engel[1]**, **Barbara Wohlmuth[3,4]**, **David Labat[5]**, and **Gabriele Chiogna[1,6]**

[1]Chair of Hydrology and River Basin Management, Technical University Munich, Munich, Germany, [2]Department for River Basin Management, Erftverband, Bergheim, Germany, [3]Chair for Numerical Mathematics, Technical University Munich, Munich, Germany, [4]Department of Mathematics, University of Bergen, Bergen, Norway, [5]Geosciences Environnement Toulouse – GET, Toulouse, France, [6]Institute of Geography, University of Innsbruck, Innsbruck, Austria

Abstract Global sensitivity analysis is an important step in the process of developing and analyzing hydrological models. Measured data of different variables are used to identify the number of sensitive model parameters and to better constrain the model output. However, data scarcity is a common issue in hydrology. Since in hydrology we are dealing with multi-scale time dependent problems, we want to overcome that issue by exploiting the potential of using the decomposed wavelet temporal scales of the discharge signal for the identification of sensitive model parameters. In the proposed methodology, we coupled the discrete wavelet transform with a technique for model parameter dimension reduction, that is, the active subspace method. We apply the proposed methodology to the LuKARS model, a lumped karst aquifer model for the Kerschbaum spring in Waidhofen/Ybbs (Austria). Our results demonstrate that the temporal scale dependency of hydrological processes affects the structure and dimension of the active subspaces. The results reveal that the dimensionality of an active subspace increases with the increasing number of hydrologic processes affecting a temporal scale. As a consequence, different parameters are sensitive on different temporal scales. Finally, we show that the total number of sensitive parameters identified at different temporal scales is larger than the number of sensitive parameters obtained using the complete spring discharge signal. Hence, instead of using multiple time series to determine the number of sensitive parameters, we can also obtain more information about parameter sensitivities from one single, decomposed time series.

1. Introduction

Uncertainty quantification and model diagnostics are important components of hydrological modeling (Hartmann et al., 2017; Melsen & Guse, 2021; Schwemmle et al., 2021; Wagener & Pianosi, 2019). Quantifying parametric uncertainty is important since the reliability of simulation results strongly depends on the parametrization of a model (Beven, 1995; Reinecke et al., 2019). Diagnostic model analyses are helpful to investigate parameter and process dynamics as well as to better understand process representations in hydrological models (Guse et al., 2016; Pfannerstill et al., 2015). The problem of equifinal parameter sets is well known in hydrology (Beven, 2006; Her & Chaubey, 2015; Kelleher et al., 2017) and time series of different variables (e.g., discharge, groundwater levels, and snow depth) can be used to constrain model parameters according to the physical processes that they describe (Efstratiadis & Koutsoyiannis, 2010; Kollat et al., 2012; Tuo et al., 2018; Vrugt et al., 2003). However, data scarcity often prevents the practical application of this approach and motivates the search for new methods to better identify sensitive model parameters, which is the focus of this work. Sensitivity analysis measures how much the output of a model, for example, discharge, changes by varying the model inputs and parameters (Wagener & Montanari, 2011; Werkhoven et al., 2008). Sensitivity analysis methods can be divided into two groups: local and global methods (Pianosi et al., 2016; Saltelli et al., 2008). In a local sensitivity analysis, parameter modifications are only performed at single locations in the parameter space (Saltelli et al., 2019; Tang et al., 2007). In contrast, in a global analysis, parameter sensitivity is measured over the full parameter space (Razavi & Gupta, 2015; Song et al., 2015). Global methods are usually preferred in hydrology as they consider uncertainties due to

combinations of parameters throughout the admissible parameter space (Cloke et al., 2008; Smith, 2013; Wagener & Pianosi, 2019).

Constantine et al. (2014) and Constantine and Diaz (2017) proposed the active subspace method as a tool to perform global sensitivity analysis and for model parameter dimension reduction. To identify an active subspace, we seek orthogonal directions in the space of parameters in which the gradient of a data misfit function, that is, an evaluation function between observed and simulated discharge, varies most. These dominant directions span the subspace and define a new coordinate system in a lower dimensional space (Teixeira Parente, Bittner, et al., 2019). Besides computing a global sensitivity metric, this method has the advantage that it further provides information on relevant linear combinations of model parameters. These relevant parameter combinations can be used to efficiently construct surrogate models that mimic the behavior of a hydrological model at low computational costs (Erdal & Cirpka, 2019; Teixeira Parente, Mattis, et al., 2019). The active subspace method has been successfully applied in several hydrological studies ranging from lumped models (Teixeira Parente, Bittner, et al., 2019) to distributed modeling approaches (Erdal & Cirpka, 2020; Gilbert et al., 2016). Bittner, Teixeira Parente, et al. (2020) also showed that the structure and dimension of an active subspace can find a reasonable explanation for dominant hydrological processes and catchment characteristics, in case of a lumped karst hydrological model. So far, the active subspace method has been applied to hydrological variables that integrate processes occurring at multiple temporal scales, such as discharge and heat fluxes (Erdal & Cirpka, 2020; Jefferson et al., 2015). However, it is well known that hydrological time series can be decomposed into different temporal scales, for example using the wavelet transform analysis (Grinsted et al., 2004; Labat et al., 2000b; Torrence & Compo, 1998).

Wavelet transforms can be described as time scale analysis that allows us to detect changes in the frequency components of a signal characterized by some intermittency. They are used to determine the crucial scales of variability of a time series. Furthermore, wavelet transforms are commonly applied to localize changes in the modes of variability within a time series, in particular when signal fluctuations are highly non-stationary and physical processes operate under a large range of scales. For example in hydrology, flood processes operate on temporal scales ranging from hours to days, whereas long term climate forcings affect hydrological processes on temporal scales larger than years (Labat, 2005). The works of Daubechies (1990), Grinsted et al. (2004), Sang et al. (2013), and Torrence and Compo (1998) offer an excellent introduction to the continuous and discrete wavelet transform and their application in natural sciences. Focusing on hydrology, wavelet transforms have been applied for time series analysis (Carey et al., 2013; Coulibaly & Burn, 2004; Labat, 2005; Labat et al., 2000b; Marcolini et al., 2017; Nalley et al., 2012), to study the coherence between hydrological variables and climatic and meteorological drivers (Jennings & Jones, 2015; Massei et al., 2010; Nalley et al., 2016; Schaefli et al., 2007), to identify the impact of anthropogenic activities on the hydrological cycle (Pérez Ciria et al., 2019; Zolezzi et al., 2009), to perform catchment classification (Agarwal et al., 2016; Pérez Ciria & Chiogna, 2020), to perform stochastic simulations of precipitation or discharge time series (Brunner & Gilleland, 2020; Hörning & Bárdossy, 2018; Nowak et al., 2011) and change point analysis (Adamowski & Prokoph, 2014). Less common is the application of wavelets for the assessment of model performance (Chiogna et al., 2018; Rathinasamy et al., 2014) and model calibration (Duran et al., 2020; Schaefli & Zehe, 2009). To the best of our knowledge, wavelets have not yet been applied in the context of model parameter sensitivity analysis.

Therefore, we aim to investigate if different temporal scales of a modeled discharge signal are sensitive with respect to different hydrologic model parameters. Notice that investigating parameter sensitivities on different temporal scales is very different from investigating temporally varying parameter sensitivities (Massmann et al., 2014; Pfannerstill et al., 2015). In fact, we are not investigating how model parameter sensitivities change over time but how their sensitivity is distributed over different temporal scales. Our hypothesis is that the active subspace dimension reflects how different linear combinations of model parameters control the simulated hydrological processes on multiple temporal scales. Moreover, we hypothesize that the sensitive parameters differ for different temporal scales of the signal, and that they can be directly related to the dominant hydrological processes of the respective temporal scales. We expect that quickflow components can be identified on low temporal scales (in the order of days) by means of the model parameters that control these hydrological processes. The opposite occurs for the slowflow components, that is, the diffusive groundwater recharge and the baseflow, which we expect to identify mostly on high temporal
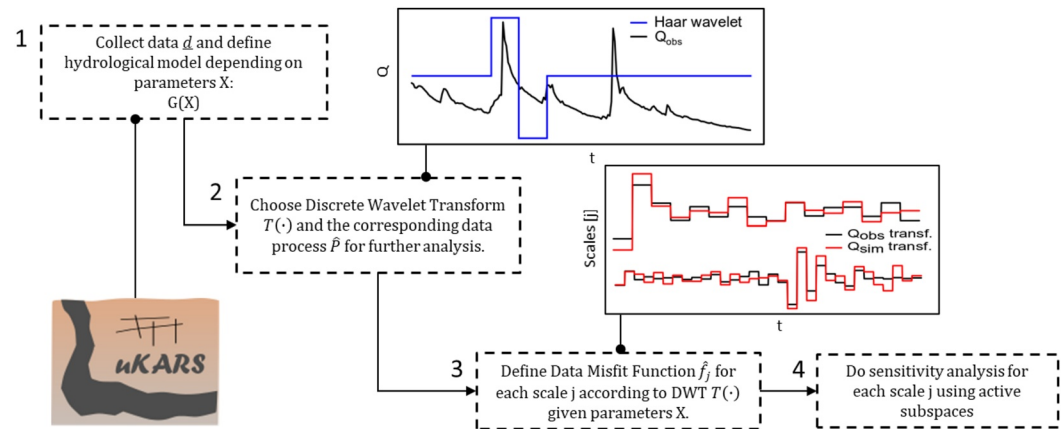
Figure 1. Flowchart of the methodology for coupling the active subspace method with the discrete wavelet transform.

scales (in the order of weeks to years). To test these hypotheses, we couple the active subspace method with the discrete wavelet transform (DWT). DWT is an orthogonal wavelet transform and the original time series can be reconstructed by deconvolution. In the continuous wavelet transform (CWT), on the contrary, the reconstruction of the original signal is complicated by the redundancy of the coefficients in time and temporal scale. Performing a sensitivity analysis of coefficients which are redundant, and hence correlated across time and scale, is highly non-trivial.

We apply the proposed methodology to a lumped karst aquifer model, that is, LuKARS (Land use change modeling in KARSt systems), using data from the Kerschbaum springshed in Austria (Bittner et al., 2018; Bittner, Rychlik, et al., 2020). We use the same data set as used in Teixeira Parente, Bittner, et al. (2019), who performed sensitivity analysis using the active subspace of the spring discharge, that is, the discharge measured at the Kerschbaum spring. This allows us to compare the results obtained from the temporal scale-dependent sensitivity analysis with those obtained using the entire discharge signal. In Section 2, we provide details about the mathematical framework for coupling the active subspace method with DWT as well as a short description of the LuKARS model and data used. In Section 3, we show how the sensitivities of LuKARS model parameters vary over different temporal scales and how they are linked to the dominant hydrological processes in the Kerschbaum spring. Moreover, we highlight that sensitive parameters can be hidden in the temporal scales of a spring discharge that are not identified as sensitive when considering the complete discharge signal. Finally, we summarize our findings in Section 4.

2. Methodology

The idea of this study is to perform an independent sensitivity analysis for each temporal scale of a modeled quantity of interest. Therefore, the methodology that we present aims at decomposing both, the modeled and the measured discharge signal at different scales using DWT. In order to guarantee the independence of sensitivity scores for each temporal scale, the chosen measurement error model has to be transformed such that the resulting scale-errors can be considered independent. Then, we test if the dimension and structure of the active subspaces, that is, the sensitive model parameters, are different among different scales. Our goal is to identify if different temporal scales of the modeled discharge signal are sensitive to different model parameters. If so, we want to investigate if these scales can be approximated by an active subspace with different dimensions and eigenvectors. This entire process is summarized in Figure 1. For reproducibility, the codes and data of the methodology can be downloaded from Bittner, Engel, et al. (2020).

2.1. Coupling DWT With Active Subspaces

In the following, we provide a detailed explanation of how we couple the DWT with the active subspace method. For convenience, matrices, and vectors are denoted by bold letters. Scalars and sets are not indicated with a bold letter. If the output of a function G of a quantity $\bullet$ is a matrix, it is indicated as $\mathbf{G}(\bullet)$. We do

this analogously for vectors, scalars and sets. A quantity, for example, discharge time series, is considered as transformed if it was decomposed from the original to the wavelet basis. To distinguish between original and transformed quantities, $\tilde{\bullet}$ is introduced as the transformed quantity and $\hat{\bullet}$ as the approximated version of $\tilde{\bullet}$ within the transformed wavelet basis.

2.1.1. Discrete Wavelet Transform

The starting point of this methodology is to define a hydrological model $G(X)$, in our case LuKARS, and to collect time series data $\mathbf{d}$ that should be simulated by the model, here the discharge of the Kerschbaum spring (Step 1 in Figure 1). Notice, however, that the proposed methodology is general and can be applied to other lumped or distributed models and other quantities of interest. Then, the next step is to choose a DWT (Step 2 in Figure 1), that is, a mother wavelet, and decompose the measured and simulated discharge time series into several temporal scales. Our measured discharge time series $\mathbf{d}$ consists of n data points. The natural frequency of discrete wavelet transforms is two (Walnut, 2013). Hence, n is chosen as

$$n = 2^m, \tag{1}$$

where $m \in \mathbb{N}$. A scale j is defined as the details coefficients $\tilde{d}_j$ corresponding to the $(m - j)$-th iteration in a filter bank (Mallat, 1989). A filter bank is a bandpass filter that separates an input time series, for example, spring discharge, into multiple components with distinguishable frequencies of the original signal. The filter bank recursively splits the given time series in the details and approximation coefficients $\tilde{a}_j$ as defined in Walnut (2013). This means that the details coefficients of scale j are obtained by decomposing the approximation coefficients of scale $(j + 1)$. In total, we have $(m + 1)$ scales. Accordingly, we define $T(\bullet)$ as the DWT of the measured and modeled discharge time series:

$$\tilde{d}_j = T_j(\mathbf{d}) \ \forall j = 0\ldots m. \tag{2}$$

The transformation T gives a set of details coefficients with m members and one approximation coefficient $\tilde{a}_0$ which is referred to as the details coefficient of Scale 0 $\tilde{d}_0$ for the sake of simplicity. Hence, the subscript j chooses a member of the set given by T: the scale j of the transformed discharge. Thus, the decomposition of the simulated output from the hydrological model G into its temporal scales can be written as

$$\tilde{G}_j = T_j(G). \tag{3}$$

2.1.2. Definition of the Data Misfit Function for Different Scales

The decomposition of the measured and modeled discharge time series is the most important part in our methodology since the sensitivity has to be quantified with respect to the gradient of a data misfit between measured and simulated discharge for each scale independently. Thus, to perform a sensitivity analysis of each scale with respect to the data misfit we need an evaluation function for each scale. Similar to Teixeira Parente, Bittner, et al. (2019), we define the Data Misfit Function (DMF) between the measurements d and the simulated discharge $G(X)$ with a set of model parameters X as

$$f(X) = \frac{1}{2} \left\| \Gamma^{-\frac{1}{2}} (d - G(X)) \right\|_2^2, \tag{4}$$

where $\|\bullet\|_2^2$ is the square of the Euclidean norm.

The DMF in Equation 4 is a squared error function weighted by a matrix $\Gamma^{-\frac{1}{2}}$. In contrast to the Nash-Sutcliffe Efficiency (Nash & Sutcliffe, 1970), which is a nonweighting squared error function favoring high-flow conditions, the DMF gives a relative error between model results and observations and does not focus on low- or high-flow conditions. In this work, an additive Gaussian measurement noise is used. Hence, the exponential of $f(X)$ is equal to the unnormalized $\mathcal{N}(d, \Gamma)$. Accordingly, since the data is discrete in time, it can be modeled as a discrete Gaussian Process $GP(d)$ with covariance matrix Γ and mean vector d. Here, Γ is a diagonal matrix describing an homoscedastic error of the measured time series. Here, we consider an error of the measured discharge of $2 \ \mathrm{ls}^{-1}$. The advantage and the limitations of this assumption will be discussed in Section 3.5.

The construction of the DMFs within the wavelet basis requires the definition of the mean vector d_j and covariance matrix Γ_j for each scale j. Considering that the measured values and their wavelet transform

are uncertain, we need to ensure that the DWT of the original signal properly distributes this uncertainty among each scale. As a consequence, coupling the active subspace method with DWT requires transformation of the random process as a whole in order to properly define a DMF $\tilde{f}_j(X)$ for each scale j (Step 3 in Figure 1). The idea is to find a mother wavelet (Step 2 in Figure 1) such that the scales can be considered statistically independent from each other. By that, we ensure obtaining independent information about the sensitivity of the parameters from each scale without any loss of information about the uncertainty in the measurements.

To sum up, we aim at obtaining zero covariance between the wavelet coefficients of different scales. In case this condition is not satisfied, we may have a loss of information in the transformation process. The term information is used in a Shannon Entropy sense (Shannon, 1948). As a measure for this information loss, we introduce the Kullback-Leibler-divergence of the whole transformed process in the wavelet domain $\tilde{P}$ and the lumped process $\hat{P}$, in which the scales are assumed to be independent. We refer to this as the Wavelet Mutual Information (*WMI*), since the idea is based on the approaches for obtaining the Mutual Information (*MI*) of random variables as described in Cover and Thomas (2012):

$$WMI(\tilde{P}) := D_{KL}(\tilde{P}\|\hat{P}). \tag{5}$$

As $\tilde{P}$ and $\hat{P}$ are discrete processes, it is feasible to model them as multivariate probability density functions. Hence, the *WMI* for a discrete Gaussian scale process $\widetilde{GP}$ can be obtained by inserting the definition of a multivariate Gaussian into Equation 5:

$$WMI\left(\widetilde{GP}(\boldsymbol{d})\right) = \frac{1}{2}\left(ln\left(\frac{\det \hat{\boldsymbol{\Gamma}}}{\det \tilde{\boldsymbol{\Gamma}}} \right) + tr\left(\tilde{\boldsymbol{\Gamma}}\hat{\boldsymbol{\Gamma}}^{-1} - \boldsymbol{I} \right) \right), \tag{6}$$

where $\boldsymbol{I}$ is the identity. If the WMI is equal to 0, we do not loose any information by assuming independent scales. Accordingly, we look for a transformation T of the measurement data $\boldsymbol{d}$ with a constant Gaussian error, such that

$$WMI\left(T\left(GP(\boldsymbol{d})\right)\right) = 0 \tag{7}$$

or that the dependence error is as small as possible. Having this transformation T, we define the new DMFs for each scale $\tilde{f}_j$ with respect to the corresponding random process $\tilde{P}_j$ and obtain statistically independent scales.

As it can be shown (see Text S1 in Supporting Information S1), the Haar-Wavelet yields that the WMI computes to 0 for homoscedastic Gaussian errors. Thus, we choose the Haar-Wavelet as our mother wavelet. Nevertheless, it is important to note that for an heteroscedastic error, for example, a non-constant diagonal covariance matrix $\boldsymbol{\Gamma}$, the *WMI* might be small but does not compute to 0 - even for the Haar system. For that reason, we choose a homoscedastic measurement error of $2\,\mathrm{ls}^{-1}$ for the proposed methodology.

For the Haar-Wavelet, the set of new DMFs $\hat{f}$ can be looked at as $\tilde{f}$, since all computations are exact and no information is lost. Hence, they can be defined for each scale j (Step 3 in Figure 1) as follows:

$$\tilde{f}_j(X) = \frac{1}{2} \left\| \tilde{\boldsymbol{\Gamma}}_j^{-\frac{1}{2}} (\tilde{\boldsymbol{d}}_j - \tilde{\boldsymbol{G}}_j(X)) \right\|_2^2, \tag{8}$$

where $\tilde{\boldsymbol{\Gamma}}_j$ is the covariance matrix for scale j. Note that the approach shown in this paper can be done for every basis function that supports a decomposition as given in Equation 2.

2.1.3. Active Subspaces for Sensitivity Analysis Within Different Scales

Now that we obtained $\tilde{f}$ and $\tilde{G}$, we conduct the sensitivity analysis using the Active Subspace method exactly as in Teixeira Parente, Bittner, et al. (2019). The only difference is that we do the analysis for the $m + 1$ corresponding decomposed DMFs and model outputs as input (Step 4 in Figure 1). Accordingly, the Active Subspace method gives the eigenvectors $\boldsymbol{v}_{j,k}$ of a gradient matrix $\boldsymbol{C}_j$ for each scale j defined as follows:

$$\boldsymbol{C}_j = E[\nabla_X \tilde{f}_j(X)\nabla_X \tilde{f}_j(X)^T] = \boldsymbol{W}_j \boldsymbol{\Lambda}_j \boldsymbol{W}_j^T, \tag{9}$$

where $\boldsymbol{W}_j = [\boldsymbol{v}_{j,1} \dots \boldsymbol{v}_{j,n}]$ and $\boldsymbol{\Lambda}_j = diag(\lambda_{j,1} \dots \lambda_{j,n})$ having $\lambda_{j,k} \geq \lambda_{j,k+1}$. The first index j is the scale and the second denotes the eigenvector k.

Thus, the eigenvalues $\lambda_{j,k}$ are a measure for the sensitivity of the scale DMF $\tilde{f}_j$ with respect to the corresponding eigenvectors $\mathbf{v}_{j,k}$. The scale sensitivity score $s_{j,i}$ of parameter x_i within scale j is calculated by

$$s_{j,i} = \sum_{k=1}^{K} \lambda_{j,k} v_{j,k,i}, \tag{10}$$

where K is the number of parameters and i denotes the parameter. Note that $s_{j,i}$ is not the global total sensitivity. It is solely global within scale j. For accessing the global total measure, a weighting of the gradient of the scale DMF with respect to its contribution to the gradient of the total DMF would be necessary. However, no weighting is considered in this work since our intention is to use the entire signal of the discharge for the wavelet decomposition to obtain an independent information for each time scale.

2.2. Kerschbaum Spring LuKARS Model

The Kerschbaum springshed is located close to the city of Waidhofen/Ybbs in Austria (Figure 2a). The recharge area of the mainly dolomitic karst system covers about 2.5 km^2 and can be considered as a small scale, pre-alpine catchment. Figure 3 classifies the behavior of the Kerschbaum spring by means of statistical and spectral indices. The cross-correlation between precipitation and spring discharge, shown in Figure 3a, highlights a quick response to precipitation events after 1 day with the highest correlation coefficient r_{xy} of 0.37. Moreover, we can identify a quick decrease of r_{xy}, pointing toward a rapid propagation of the input signal (precipitation) through the aquifer (Labat et al., 2000a; Mangin, 1984). In the cross-correlation as well as in the spectral density (Figure 3b), we can identify a sudden change in slope from 2.35 to 1.32 after 8 days. This change points toward an activation of drainage from the aquifer storage, that is, baseflow (Larocque et al., 1998). More information about the study site are provided by Bittner et al. (2021) and Narany et al. (2019).

The LuKARS model was developed by Bittner et al. (2018) to investigate how mining activities in the recharge area affect the quantity of discharge in the Kerschbaum spring. A GUI for the model is available as open source plugin for FREEWAT (Rossetto et al., 2018) in QGIS (Bittner, Rychlik, et al., 2020). The model is based on the implementation of hydrotopes, that is, areas with homogeneous soil and land use characteristics (Arnold et al., 1998), shown in Figures 2a and 2b. Determined by its individual physical characteristics, each hydrotope shows a distinct response to an input event, for example, precipitation or snow melt. All hydrotopes simulate three types of flow (Figure 2b), that is, quickflow through conduits, groundwater recharge and secondary spring discharge, which are controlled by hydrotope-specific parameters (Figure 2c). They all share one common baseflow storage, that is, the saturated zone, to which the recharge is transferred (Bittner et al., 2018). The sum of all hydrotope quickflow responses at a given time step represents the conduit flow in the recharge area. Then, the sum of the integrated hydrotope quickflows and the baseflow simulate the spring discharge. The equations of the LuKARS model are provided in Text S2 in Supporting Information S1. The model parameter ranges used in this study are shown in Table 1. In the specific case of the minimum and maximum storage values of a hydrotope, that is, E_{min} and E_{max}, parameter ranges were obtained using the methodology suggested by the German Association for Water, Wastewater and Waste (DWA, 2020). The ranges of all other model parameters were chosen as proposed by Teixeira Parente, Bittner, et al. (2019) and the solution of the Bayesian inversion model found in that work supports this choice. Further, we use daily data for precipitation, temperature, snow depth and spring discharge in the period from January 2006 to December 2008 to run the model. The data was kindly provided by the water works Waidhofen/Ybbs. It is important to note that, in order to apply the active subspace method, all model parameters need to be independent from a statistical point of view. However, in LuKARS the parameters within one hydrotope can be related to each other. Moreover, the parameters of one hydrotope are also dependent on the parameters of other hydrotopes, as shown in Text S3 Supporting Information S1. Therefore, we follow the framework proposed for the Kerschbaum LuKARS model in Teixeira Parente, Bittner, et al. (2019) and transform the model parameters into statistically independent calibration parameters. Independence is achieved by replacing a model parameter, for example, $E_{max,i}$, by a calibration parameter, that is, $\Delta E_{min,i}$, which is the difference between $E_{max,i}$ and the dependent model parameter, that is, $E_{min,i}$. For the sake of completeness, we include this methodology in Text S3 in Supporting Information S1. Since this transformation does not have an impact on the interpretation of the results shown in the following section, it will not be further discussed.
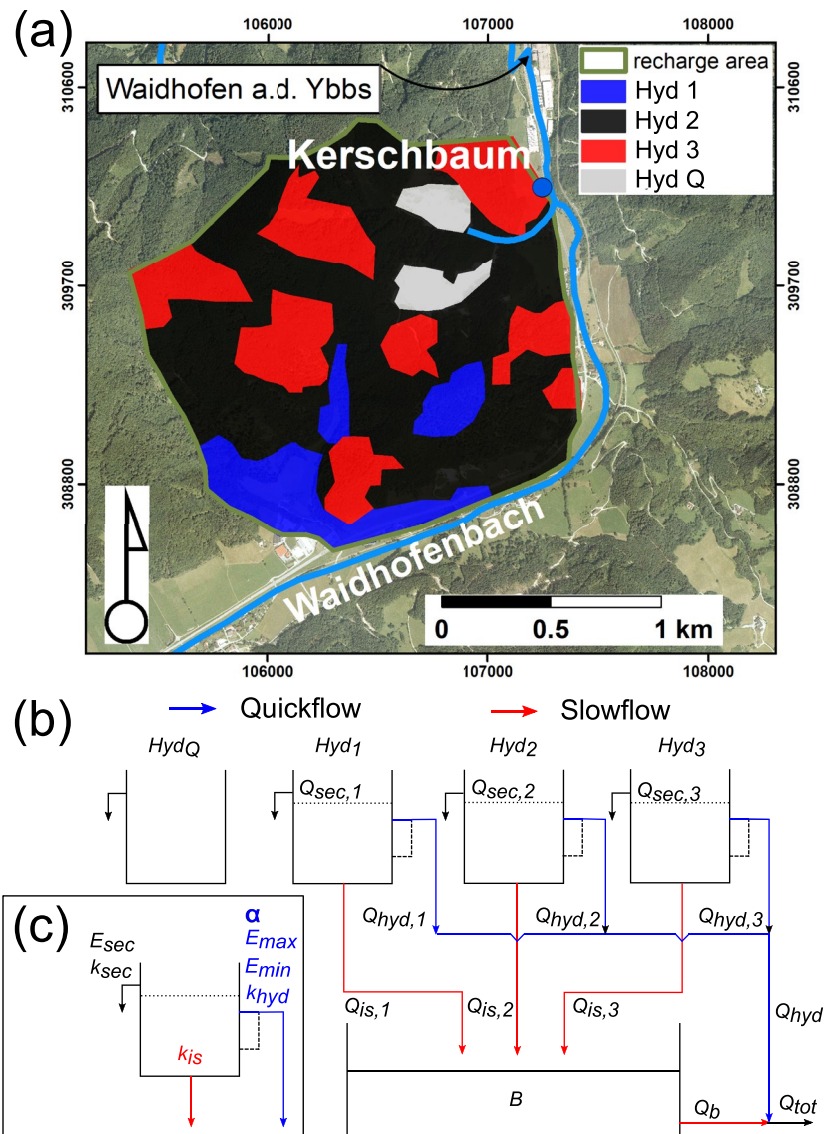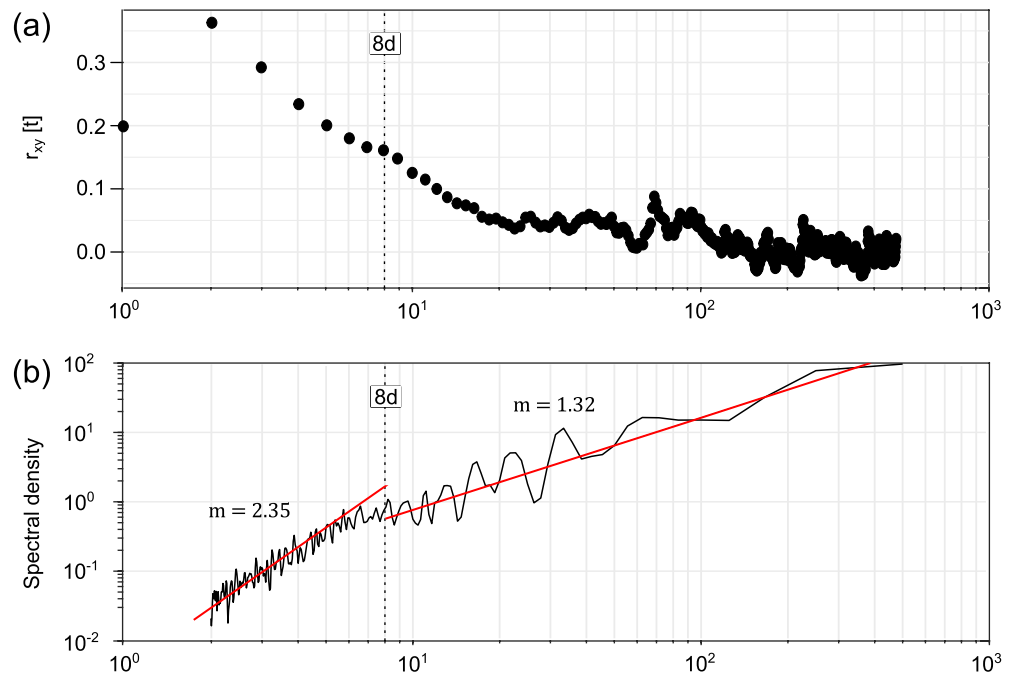
Figure 2. (a) Recharge area of the Kerschbaum spring close to Waidhofen/Ybbs (Austria) including the distribution of hydrotopes, that is, Hyd 1 (13% of recharge area), Hyd 2 (56% of recharge area), Hyd 3 (27% of recharge area), and Hyd Q (4% of recharge area). The orthophoto was kindly provided by the waterworks owner in Waidhofen/Ybbs. (b) The concept of LuKARS including conceptual representation of the quickflow and slowflow processes. (c) The structure of a LuKARS hydrotope including the model parameters to highlight which processes (quickflow and slowflow) are controlled by which parameters. The explanation for the abbreviations is provided in Text S2 in Supporting Information S1.

3. Results and Discussion

In the following section, we describe and discuss the results obtained by applying our methodology to the Kerschbaum LuKARS model. More precisely, we focus on the dimensions of active subspaces on different scales (i.e., the number of relevant eigenvalues), the scale structures of the different eigenvectors as well as the hydrological meaning of identified scale dependencies. In the following, the order of scales is from the lowest to the highest frequency. Scale 1 represents the lowest frequency, that is, 1,024 days, and Scale 10 the highest frequency, that is, 2 days. Finally, Scale 0 represents the mean of the discharge signal.

Figure 4 shows how precipitation (Figure 4a) and snow melt (Figure 4b) affect the discrete wavelet scales of the Kerschbaum spring discharge (Figure 4c) as well as the complete discharge signal (Figure 4d). Please

Figure 3. Time series analysis of the Kerschbaum spring discharge. (a) The cross-correlation between precipitation and spring discharge, highlighting a quick response of 1 day lag time and storage effects after 8 days. (b) The spectral density of the discharge signal, also highlighting an abrupt change in spectral density of variance after 8 days, indicated by a change in slope from $m = 2.35$ to $m = 1.32$.

note that Figure 4c does not display the values on the y-axis because they are not relevant for the following qualitative interpretation. As an example, we highlight four significant peak discharges with gray colored frames in the background. These fast spring discharges happened in response to major snow melt, for example, April 26, 2006, or precipitations events, for example, June 2, 2006 and August 7, 2006. In the DWT scales (Figure 4c), we can observe that major input events have an effect on the spring discharge from 2 days up to a period of 8 days, which is similar to what we identified in the cross-correlation and spectral analysis (Figure 3). Very intense input events, such as the precipitation event on September 6, 2007, can affect even more temporal scales, up to 64 days. This is consistent for example with the observations of Schaefli et al. (2007) and other works in the literature (Charlier et al., 2015; Yang et al., 2012) and shows that when we decompose the hydrologic signal among multiple temporal scales, high-flow conditions have an impact on scales larger than the event duration.

Table 1
*Overview of the Model Parameter Ranges Defined for all Hydrotopes*

Hydrotope	$k_{hyd} (m^2 d^{-1})$	E_{min} (mm)	E_{max} (mm)	α (−)	k_{is} (m mm^{-1}d^{-1})	k_{sec} (m mm^{-1}d^{-1})	E_{sec} (mm)
Description	Discharge coefficient quickflow	Minimum storage capacity	Maximum storage capacity	Quickflow exponent	Discharge coefficient recharge	Discharge coefficient second springs	Activation level second springs
Hyd 1	9–900	10–50	15–75	0.7–1.6	0.002–0.2	0.0095–0.95	25–70
Hyd 2	8.5–850	40–80	80–160	0.5–1.3	0.00055–0.055	0.0023–0.23	130–220
Hyd 3	7.7–770	75–120	155–255	0.2–0.7	0.00025–0.025	0.0015–0.15	320–450

Note. The respective numbers indicate the lower bound and the upper bound of the parameter ranges used as prior intervals. For the meaning of the parameters, we refer to the explanation given in Text S2 in Supporting Information S1.
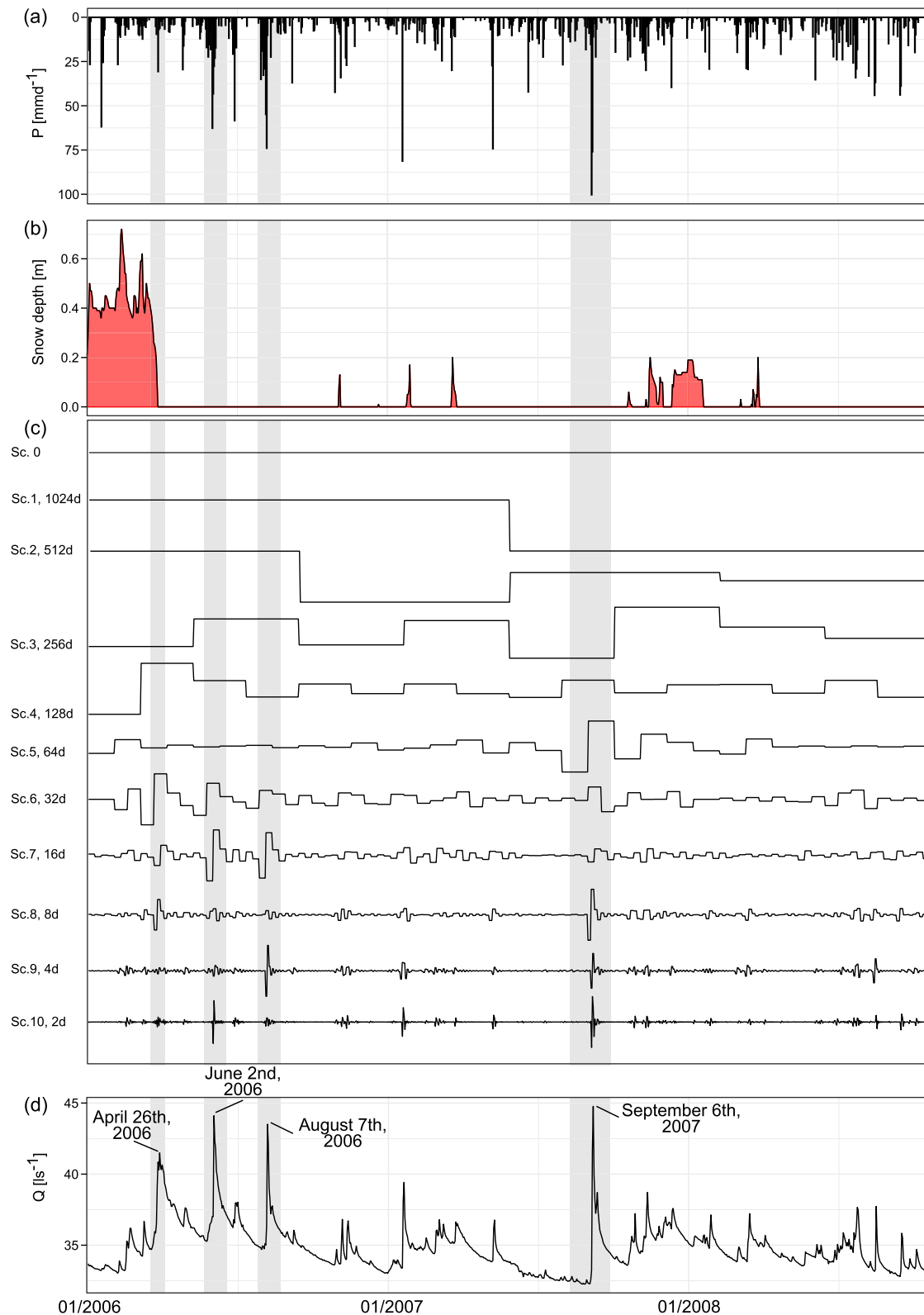
Figure 4. Data time series used in the LukARS model for the period of interest from 2006 to 2008 and the discrete wavelet scales of the measured discharge time series. (a) Precipitation, (b) measured snow depths, (c) the discrete wavelet scales (Sc.) of the Kerschbaum spring discharge signal, and (d) the Kerschbaum spring discharge time series. The gray bars highlight specific peak flow events during the period of interest. Note that Scale 10 represents the highest frequency, that is, 2 days, whereas Scale 1 represents the lowest frequency, that is, 1,024 days.
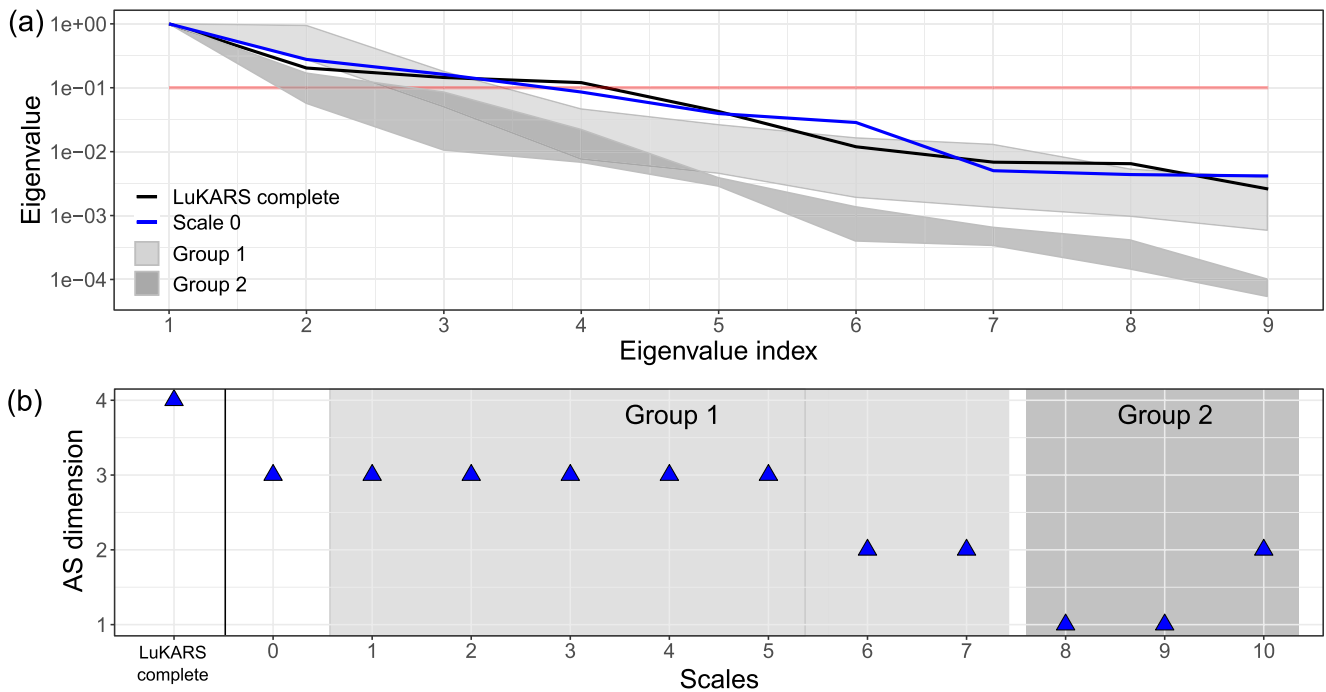
Figure 5. Active subspace dimensions. (a) Eigenvalue decay of both scale groups, that is, Group 1 representing Scale 1 to 7 and Group 2 representing Scale 8 to 10, Scale 0 and "LuKARS complete" normalized to the maximum eigenvalue of each scale. The horizontal red line indicates the truncation level above which the active subspace is defined. (b) Active subspace dimension of each discrete wavelet scale grouped in both groups of scales. "LuKARS complete" shows the active subspace dimension when applying the active subspace method to the Kerschbaum LuKARS model without the DWT.

3.1. Scale Dependence of Active Subspaces

Figure 5a shows the decay of the eigenvalues of each wavelet scale (Equation 9) over the first nine eigenvalues and the truncation level. Based on our findings from the cross-correlation, spectral analysis and the DWT, we can distinguish between two groups of scales highlighted in Figures 5a and 5b. Group 1 represents the sub-monthly to superannual scales, that is, Scale 1 to Scale 7. Group 2 represents the sub-weekly to weekly, that is, Scale 8 to Scale 10. The lower frequencies (Group 1) have active subspace dimensions between 2 and 3. In comparison, the sub-weekly to weekly scales (Group 2), representing faster spring discharge responses (Figure 4c), only have active subspace dimensions between 1 and 2. We decided to truncate an active subspace after an eigenvalue decay over one order of magnitude. This choice, although arbitrary, does not affect the main outcomes of the analysis as discussed by Teixeira Parente, Bittner, et al. (2019). The eigenvalues are normalized to the maximum eigenvalue of each scale to allow for comparability of decays between each scale. When looking at the eigenvalue decay of each scale (Figure 5a), we can identify that Scale 0 shows the weakest decay of all scales. Moreover, we find that with an increasing wavelet scale, the eigenvalues decay faster. The dimension of the active subspaces identified for both Group 1 and Group 2 are lower when compared to the original active subspace of the Kerschbaum LuKARS model computed without the DWT, that is, 4 (also shown in Figure 5b). The fact that each wavelet scale has a low dimensional active subspace indicates that fewer eigenvectors are sensitive and informed.

3.2. Eigenvector Structures on Different Scales

In Figure 6, we show the first three eigenvectors of the complete LuKARS model (Bittner et al., 2018) and one representative scale for each group, that is, Scale 1 for Group 1 and Scale 8 for Group 2. In the relevant eigenvectors of the complete LuKARS model (Figure 6a), we can observe a strong contribution of the discharge coefficient of groundwater recharge from each hydrotope, that is, k_{is}. Moreover, we see that Hyd 2 has the highest contribution, which is the largest hydrotope in the recharge area (see Figure 2a). The second highest contribution comes from Hyd 1, representing the most dynamic hydrotope in terms of discharge variability. Although the area of Hyd 3 is larger than Hyd 1 (Figure 2a), its contribution to the first
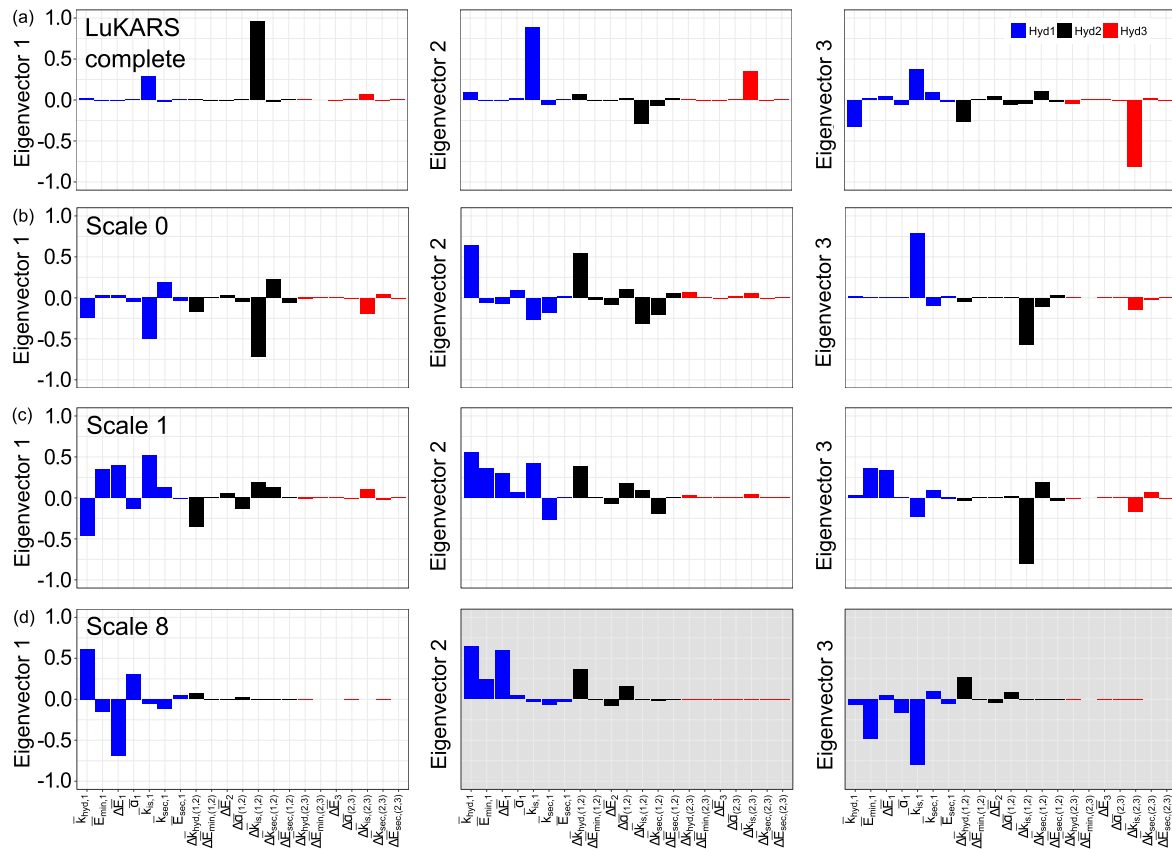
Figure 6. Eigenvectors of different scales. (a) First three relevant eigenvectors of the complete LuKARS model computed without scale decomposition. (b) First three relevant eigenvectors of Scale 0. (c) First three relevant eigenvectors of Scale 1. (d) First three eigenvectors of Scale 8. The gray shaded eigenvectors are not relevant as identified from the eigenvalue decay but are shown for completeness.

eigenvector is weakest. When further taking into account Eigenvectors 2 and 3, a similar pattern in terms of contributing hydrotopes can be observed, that is, Hyd 1 and Hyd 2 are dominant. It can be seen that k_{hyd} of Hyd 1 and 2, which are the discharge coefficients of the quickflow, have noticeable scores in Eigenvector 2.

Looking at the first eigenvector of Scale 0 (Figure 6b), we also find that mainly the groundwater recharge parameters (k_{is}) of each hydrotope have the highest contribution in the first eigenvector. Moreover, we can observe the same ranking of hydrotope contributions in the first eigenvector compared to the complete LuKARS model, that is, in decreasing order Hyd 2, Hyd 1, and Hyd 3. When further taking into account Eigenvector 2 and 3, we further notice high scores of the quickflow parameters k_{hyd} of Hyd 1 and Hyd 2.

Next, we look at the eigenvectors of Scale 1, being representative for the scales of Group 1. In all eigenvectors (Figure 6c), we can observe a dominant contribution of Hyd 1 and Hyd 2 parameters, similar to Scale 0. In contrast to Scale 0, Hyd 1 parameters show a higher contribution as compared to those of Hyd 2. When looking at single parameter contributions in each eigenvector, we generally observe highest scores of the discharge coefficients of k_{is} and k_{hyd} of Hyd 1 and Hyd 2. Moreover, the water storage thresholds, that is, E_{min} and ΔE (in the following referred to as the E parameters), of both dominant hydrotopes have noticeable contributions in the eigenvectors. These parameters control the onset and offset of the quickflow and, thus, further control the amount of water becoming groundwater recharge.

Although we are showing the first three eigenvectors of Scale 8 (Figure 6d), only the first eigenvector is relevant as highlighted by the active subspace dimensions in Figure 5b. Looking at the parameters contributing to the relevant eigenvector, we notice a clear dominance of Hyd 1 parameters and neglectable scores of both other hydrotopes. In particular, k_{hyd}, the E parameters and α have the highest scores. These parameters primarily control the quickflow of Hyd 1, where α regulates the magnitude of quickflow events. In contrast
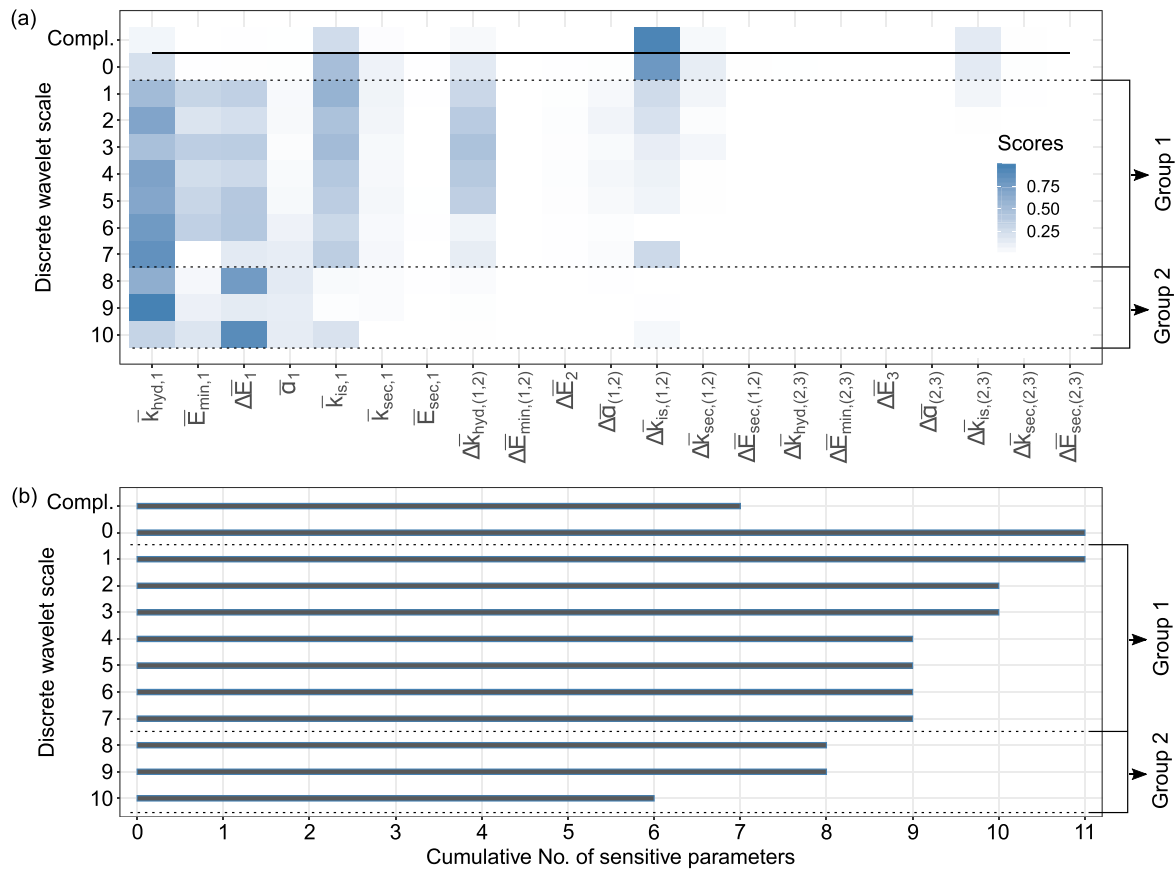
Figure 7. Scale-dependent sensitivities. Group 1 represents the sub-monthly to superannual scales and Group 2 represents the sub-weekly to weekly scales. (a) Global sensitivities shown for each model parameter and each scale. The "Compl" parameter sensitivities represent the sensitivity scores without scale dependencies. (b) Cumulative number of sensitive parameters.

to the previously discussed scales, no significant contribution from groundwater recharge controlling parameters can be noticed. These results are in good agreement with the identified impacts of snow melt and precipitation events on the temporal scales of spring discharge. As Hyd 1 has the highest quickflow variability, this hydrotope contributes most to peakflow during these events, which explains the importance of the quickflow parameters in Group 2 scales.

3.3. Scale-Dependent Parameter Sensitivities

Next, we show the parameter sensitivities computed with Equation 10 for each wavelet scale and the complete LuKARS model in Figure 7a. Both, Scale 0 and the complete LuKARS model without scale decomposition have a similar pattern in terms of sensitive parameters, comparable to our findings in the eigenvectors of the dominant eigenvalues (Figures 6a and 6b). In particular the k_{is} parameters of each hydrotope are the most sensitive parameters with decreasing scores from Hyd 2 over Hyd 1 to Hyd 3. Looking at the sensitive parameters on the sub-monthly to superannual scales (Group 1), we can observe that Hyd 1 parameters are most sensitive at all scales. Moreover, k_{is} is the most sensitive parameter of Hyd 2 with noticeable scores at all scales of Group 1. For Hyd 3, k_{is} is only sensitive at Scale 1 and 2. In general, the most sensitive parameters in the sub-monthly to superannual scales are the discharge coefficients of the quickflow, that is, k_{hyd}, and the recharge, that is, k_{is}. Focusing on the parameter sensitivities of the sub-weekly to weekly scales (Group 2), no noticeable scores can be found in Hyd 2 and Hyd 3, with the only exception given by k_{hyd} and k_{is} of Hyd 2 at Scale 7. All sensitive parameters on these scales are related to Hyd 1, which are particularly those controlling quickflow, that is, k_{hyd}, the E parameters and α.

Figure 7b shows the total number of sensitive parameters cumulated over all discrete wavelet scales. We start cumulating sensitive parameters at Scale 10, since it has the highest frequency and represents the quickest response of the decomposed discharge signal. We define a parameter to be sensitive if its sensitivity score is larger than the 0.75-quantile of all sensitivity scores computed for each scale. In our case, this means that a parameter is sensitive if its sensitivity score is > 0.01. Parameters which are sensitive on more than one scale are counted only once in the first scale they appear. We observe that a total of 11 parameters are sensitive over all scales. In comparison, in the complete LuKARS model without scale dependencies, only seven parameters are sensitive. This shows that further information about sensitive parameters can be extracted from the temporal scales of the discharge. From a physical point of view, this can be explained by the temporal scale-dependent relevance of different hydrologic processes, to which different model parameters can be sensitive.

3.4. Hydrological Interpretation

In general, we found the weakest eigenvector decay for Scale 0 and decreasing active subspace dimensions with increasing wavelet scales (Figure 5). As introduced in Section 2.1, Scale 0 represents the mean of the discharge signal. From a physical point of view, the mean of the spring discharge signal represents an interplay of multiple hydrological processes, which are represented in LuKARS as quickflow and baseflow. Thus, to reproduce the mean of the discharge signal, the model also needs to consider both processes. The relevance of different hydrological processes can explain that a larger dimension of the active subspace is needed to sufficiently inform the data misfit function for the mean of the discharge signal. For faster spring responses, that is, the sub-weekly to weekly scale, we found lower dimensional active subspaces as compared to the sub-monthly to superannual scales. This finding is congruent with the results obtained by Bittner, Teixeira Parente, et al. (2020). In their synthetic test cases, they showed that spring discharge dominated by a single hydrological process displays a low dimensional active subspace (dimension between 1 and 2). However, here we did not identify such a dependence for hypothetical scenarios, but for specific temporal scales of a real spring discharge. Thus, our results highlight that the coupling between DWT and active subspaces supports identifying those temporal scales of a spring discharge to which only a small number of eigenvectors are sensitive, for example, 1 as at Scale 8. These high-frequency scales, that is, the scales of Group 2, are mainly controlled by one dominant hydrological process, for example, the quickflow from Hyd 1. Further, the coupled methodology enables identifying those temporal scales which are controlled by different hydrological processes, for example, quickflow and groundwater recharge at Scale 8. For these scales, we found higher dimensional active subspaces, for example, Three dimensions for Scale 1.

The dominant parameter contributions at Scale 0, that is, the recharge coefficient of Hyd 1, 2, and 3 (k_{is}, Figures 6b and 7a), are similar to those found in the dominant eigenvectors of the complete discharge signal (Teixeira Parente, Bittner, et al., 2019). As the major volume of the Kerschbaum spring discharge originates from baseflow (Bittner, Rychlik, et al., 2020), we argue that this is the reason why those parameters controlling the modeled baseflow, that is, k_{is} of each hydrotope, are most sensitive at Scale 0. Moreover, k_{is} of Hyd 2 is most sensitive since Hyd 2 is the largest hydrotope in the area and contributes most to the groundwater recharge. The noticeable scores of the quickflow parameters k_{hyd} at Scale 0 highlight that the mean of the discharge signal is composed of baseflow and quickflow contributions. In general, these findings highlight that the parameters in the dominant eigenvectors reflect the hydrological processes involved in producing the signal of a respective scale, here Scale 0.

In the scales of Group 1, the discharge coefficients of the groundwater recharge and quickflow (k_{is} and k_{hyd}) of Hyd 1 and Hyd 2 are most sensitive (Figures 6c and 7a). As Hyd 1 is the smallest hydrotope, this finding suggests that also on the low-frequency scales of Group 1, the discharge variability of a hydrotope can play a more significant role than the size of a hydrotope. Taking further into account that the storage parameters of Hyd 1 and Hyd 2 (E) play an important role at Scale 1, we argue that on the sub-monthly to superannual scales, both hydrological processes, the quickflow and groundwater recharge becoming baseflow, are relevant.

For scales of Group 2, we notice a clear dominance of quickflow controlling parameters, in particular the quickflow coefficient (k_{hyd}), the storage parameters (E) and the quickflow exponent (α), in the relevant eigenvector. This shows that on the sub-weekly to weekly scales, groundwater recharge and, thus, the

baseflow does not play a significant role. This interpretation is further confirmed by the cross-correlation analysis, which highlighted a dominant contribution from quickflow up to a period of 8 days (Figure 3a). Hence, our methodology shows that it is possible to identify those hydrological processes which are relevant for a respective temporal scale in the parameters of the relevant eigenvectors.

Finally, we can summarize that for Scale 0 and the sub-monthly to superannual scales, higher dimensional active subspaces are needed to reproduce the signals of these scales. This is due to the fact that different hydrological processes, for example, the quickflow and the recharge becoming baseflow, from different areas in a catchment, that is, hydrotopes, are relevant on these temporal scales. These relevant hydrological processes are reflected by the parameters contributing to each dimension of an active subspace, that is, the eigenvectors of the dominant eigenvalues. On the contrary, only small dimensional active subspaces are needed to reproduce the signals on the sub-weekly to weekly scales. This is related to the fact that only the quickflow from the hydrotope with high discharge variabilities, that is, Hyd 1, matters on that temporal scale. These findings lead us to the conclusion that, for our specific case of the LukARS model, the less complex the hydrologic process structure is on a considered scale, the lower the dimensionality of the related active subspace. Furthermore, our findings in the scale-dependent parameter sensitivities are similar to what we identified in the eigenvectors of the dominant eigenvalues shown in Figure 7a. It is interesting to observe that with an increasing scale, that is, higher frequencies, the sensitivity of the recharge coefficients k_{is} decreases. At the same time, the sensitivity of the quickflow exponent α increases. This result indicates a clear shift in the dominant hydrological processes occurring on the respective scales, since α is the parameter that controls the intensity on which quickflow occurs.

3.5. Applicability, Future Developments, and Limitations

Finally, we want to discuss the generalization of the coupled DWT—active subspace framework, its broader applicability, the usefulness of a weighting scheme for each temporal scale and limitations. The proposed methodology can be transferred to other hydrological models and find applications beyond hydrological sciences. The use of the active subspace method is particularly appealing for models with a large number of calibration parameters. The active subspace method searches for those directions in the parameter space which are most informed by data. These directions can then be used to identify an approximation of the original model with significantly lower parameter dimensions. After performing a sensitivity analysis, the active subspace method offers the advantage to do a Bayesian inversion using a surrogate model at lower computational costs (Erdal & Cirpka, 2019; Teixeira Parente, Bittner, et al., 2019). This is particularly relevant for the presented method, where an inverse problem can be defined for each temporal scale. A framework to perform a Bayesian inversion on multiple temporal scales is currently under development.

In this work, we did not give weights to the different wavelet scales, but use the entire signal of the discharge for the wavelet decomposition, such that each decomposed signal provides an independent information for the respective time scale. Providing a weight for each scale can help to reduce the risk of model overfitting by favoring specific hydrological processes which are represented by a respective temporal scale, for example, quickflow. This may be useful when we want to perform the above mentioned Bayesian inversion of model parameters using the information on sensitive parameters of each temporal scale.

By means of identified sensitive model parameters and relevant eigenvectors, our methodology can be used to infer relevant hydrological processes for different temporal scales. Inversely, if we know which hydrological processes are relevant to reasonably represent the discharge dynamics of a particular karst spring, we also can adapt the conceptual components of our model structure accordingly. Thus, we argue that our proposed methodology further contributes to the field of hydrological model diagnostics, since it can be used for model structure improvement and to verify the hydrological consistency of a conceptual model. Our approach is also novel in comparison to the one proposed for example by Pfannerstill et al. (2015) and Guse et al. (2016). In fact, our approach does not investigate time-varying parameter sensitivities, but scale-varying parameter sensitivities. The main difference between a time-varying sensitivity analysis and our temporal scale approach is related to the stationarity of parameter sensitivities. In a time-varying sensitivity analysis, parameter sensitivities are non-stationary. In contrast, in our presented approach, parameter sensitivities are stationary, since there is no change over time but only over scale. One major advantage of

our approach is that we get an integrated sensitivity for each scale over the full length of the investigated time series.

The identification of relevant hydrological processes for different temporal scales depends on the temporal resolution of the discharge time series. In our case, discharge measurements were only available with a daily resolution and, therefore, processes occurring at the subdaily scale could not be sampled. Hence, future works should also investigate those temporal scales smaller than one day to obtain a more profound understanding of the quickflow components in karstic areas.

Although we are aware that measurement errors of hydrological time series can be heteroscedastic, we consider a homoscedastic error of $2 \, \mathrm{ls}^{-1}$ for our measurement such that the WMI computes to 0. By that, we ensure not having any loss of information when decomposing our time series in the wavelet domain. The generalization of the methodology for heteroscedastic errors requires a minimization of the loss of information and a normalized version of the WMI and it is currently under development.

4. Conclusions

In the presented work, we propose a combination of an active subspace approach with the discrete wavelet transform. By that, the temporal scale dependencies of parameter sensitivities can be numerically analyzed. As benchmark setting, we apply the technology to the LuKARS lumped karst aquifer model. The obtained structure of the active subspace depends on the temporal scale for which it was identified. In particular, we identified two to three dimensional active subspaces for sub-monthly to superannual temporal scales and one to two dimensional active subspaces for the sub-weekly to weekly scales. The more hydrological processes are relevant for a temporal scale, the higher the dimensionality of the associated active subspace. For the sub-monthly to superannual temporal scales, we found that the parameters controlling the slow flowing groundwater recharge and quickflow are most important. For the sub-weekly to weekly scales, the most sensitive parameters are solely related to the quickflow of one hydrotope. Thus, the relevant linear combinations of parameters of an active subspace translate into the dominant hydrological processes for each temporal scale. Moreover, the dimensionality of an active subspace is directly linked to the complexity of the hydrologic process structure.

The proposed methodology allows us to discover hidden sensitive parameters in the spring discharge. To be more precise, we found 11 sensitive parameters when decomposing the discharge signal, whereas only seven where found with the complete LuKARS model (Figure 7b). These sensitive parameters are hidden as long as the measured discharge signal is not decomposed using the wavelet transform. Our new approach is an attractive alternative to multi-objective calibration requiring several data time series. In fact, our approach can be used to calibrate model parameters by fitting related temporal scales of the observed and simulated spring discharge. Hence, we do not require more time series to better constrain model parameters.

The presented methodology represents a novel approach toward sensitivity analysis and model diagnostics, since it allows to identify the model behavior for each temporal scale that contributes to the entire signal, for example, discharge. Moreover, the definition of a scale-dependent active subspace allows for a computationally effective application of our approach in the framework of multi-objective model calibration. We note that the active subspace method coupled with the discrete wavelet transform is quite general and not restricted to the considered example.

Data Availability Statement

References

Adamowski, J., & Prokoph, A. (2014). Determining the amplitude and timing of streamflow discontinuities: A cross wavelet analysis approach. *Hydrological Processes*, *28*(5), 2782–2793. https://doi.org/10.1002/hyp.9843

Agarwal, A., Maheswaran, R., Sehgal, V., Khosa, R., Sivakumar, B., & Bernhofer, C. (2016). Hydrologic regionalization using wavelet-based multiscale entropy method. *Journal of Hydrology*, *538*, 22–32. https://doi.org/10.1016/j.jhydrol.2016.03.023

Arnold, J. G., Srinivasan, R., Muttiah, R. S., & Williams, J. R. (1998). Large area hydrologic modeling and assessment part I: Model development. *JAWRA Journal of the American Water Resources Association*, *34*(1), 73–89. https://doi.org/10.1111/j.1752-1688.1998.tb05961.x

Beven, K. (1995). Linking parameters across scales: Subgrid parameterizations and scale dependent hydrological models. *Hydrological Processes*, *9*(5–6), 507–525. https://doi.org/10.1002/hyp.3360090504

Beven, K. (2006). A manifesto for the equifinality thesis. *Journal of Hydrology*, *320*(1–2), 18–36. https://doi.org/10.1016/j.jhydrol.2005.07.007

Bittner, D., Engel, M., Wohlmuth, B., Labat, D., & Chiogna, G. (2020). *Discrete wavelet transform coupled with the active subspace method*. HydroShare. https://doi.org/10.4211/hs.4901a0d654334c259f4ff9b49dc0a74e

Bittner, D., Narany, T. S., Kohl, B., Disse, M., & Chiogna, G. (2018). Modeling the hydrological impact of land use change in a dolomite-dominated karst system. *Journal of Hydrology*, *567*, 267–279. https://doi.org/10.1016/j.jhydrol.2018.10.017

Bittner, D., Richieri, B., & Chiogna, G. (2021). Unraveling the time-dependent relevance of input model uncertainties for a lumped hydrologic model of a pre-alpine karst system. *Hydrogeology Journal*, 1–17. https://doi.org/10.1007/s10040-021-02377-1

Bittner, D., Rychlik, A., Klöffel, T., Leuteritz, A., Disse, M., & Chiogna, G. (2020). A GIS-based model for simulating the hydrological effects of land use changes on karst systems – The integration of the LuKARS model into FREEWAT. *Environmental Modelling & Software*, *127*, 104682. https://doi.org/10.1016/j.envsoft.2020.104682

Bittner, D., Teixeira Parente, M., Mattis, S., Wohlmuth, B., & Chiogna, G. (2020). Identifying relevant hydrological and catchment properties in active subspaces: An inference study of a lumped karst aquifer model. *Advances in Water Resources*, *135*, 103472. https://doi.org/10.1016/j.advwatres.2019.103472

Brunner, M. I., & Gilleland, E. (2020). Stochastic simulation of streamflow and spatial extremes: A continuous, wavelet-based approach. *Hydrology and Earth System Sciences*, *24*(8), 3967–3982. https://doi.org/10.5194/hess-24-3967-2020

Carey, S. K., Tetzlaff, D., Buttle, J., Laudon, H., McDonnell, J., McGuire, K., et al. (2013). Use of color maps and wavelet coherence to discern seasonal and interannual climate influences on streamflow variability in northern catchments. *Water Resources Research*, *49*(10), 6194–6207. https://doi.org/10.1002/wrcr.20469

Charlier, J.-B., Ladouche, B., & Maréchal, J.-C. (2015). Identifying the impact of climate and anthropic pressures on karst aquifers using wavelet analysis. *Journal of Hydrology*, *523*, 610–623. https://doi.org/10.1016/j.jhydrol.2015.02.003

Chiogna, G., Marcolini, G., Liu, W., Pérez Ciria, T., & Tuo, Y. (2018). Coupling hydrological modeling and support vector regression to model hydropeaking in alpine catchments. *Science of The Total Environment*, *633*, 220–229. https://doi.org/10.1016/j.scitotenv.2018.03.162

Cloke, H., Pappenberger, F., & Renaud, J.-P. (2008). Multi-method global sensitivity analysis (MMGSA) for modelling floodplain hydrological processes. *Hydrological Processes: An International Journal*, *22*(11), 1660–1674. https://doi.org/10.1002/hyp.6734

Constantine, P. G., & Diaz, P. (2017). Global sensitivity metrics from active subspaces. *Reliability Engineering & System Safety*, *162*, 1–13. https://doi.org/10.1016/j.ress.2017.01.013

Constantine, P. G., Dow, E., & Wang, Q. (2014). Active subspace methods in theory and practice: Applications to kriging surfaces. *SIAM Journal on Scientific Computing*, *36*(4), A1500–A1524. https://doi.org/10.1137/130916138

Coulibaly, P., & Burn, D. H. (2004). Wavelet analysis of variability in annual Canadian streamflows. *Water Resources Research*, *40*(3). https://doi.org/10.1029/2003wr002667

Cover, T. M., & Thomas, J. A. (2012). *Elements of information theory*. John Wiley & Sons.

Daubechies, I. (1990). The wavelet transform, time-frequency localization and signal analysis. *IEEE Transactions on Information Theory*, *36*(5), 961–1005. https://doi.org/10.1109/18.57199

Duran, L., Massei, N., Lecoq, N., Fournier, M., & Labat, D. (2020). Analyzing multi-scale hydrodynamic processes in karst with a coupled conceptual modeling and signal decomposition approach. *Journal of Hydrology*, *583*, 124625. https://doi.org/10.1016/j.jhydrol.2020.124625

DWA. (2020). *Bodenhydrologische Kartierung und Modellierung*. Deutsche Vereinigung für Wasserwirtschaft, Abwasser und Abfall e.V., DWA-M 922.

Efstratiadis, A., & Koutsoyiannis, D. (2010). One decade of multi-objective calibration approaches in hydrological modelling: A review. *Hydrological Sciences Journal*, *55*(1), 58–78. https://doi.org/10.1080/02626660903526292

Erdal, D., & Cirpka, O. A. (2019). Global sensitivity analysis and adaptive stochastic sampling of a subsurface-flow model using active subspaces. *Hydrology and Earth System Sciences*, *23*(9), 3787–3805. https://doi.org/10.5194/hess-23-3787-2019

Erdal, D., & Cirpka, O. A. (2020). Improved sampling of behavioral subsurface flow model parameters using active subspaces. *Hydrology and Earth System Sciences*, *24*(9), 4567–4574. https://doi.org/10.5194/hess-24-4567-2020

Gilbert, J. M., Jefferson, J. L., Constantine, P. G., & Maxwell, R. M. (2016). Global spatial sensitivity of runoff to subsurface permeability using the active subspace method. *Advances in Water Resources*, *92*, 30–42. https://doi.org/10.1016/j.advwatres.2016.03.020

Grinsted, A., Moore, J. C., & Jevrejeva, S. (2004). Application of the cross wavelet transform and wavelet coherence to geophysical time series. *Nonlinear Processes in Geophysics*, *11*(5/6), 561–566. https://doi.org/10.5194/npg-11-561-2004

Guse, B., Pfannerstill, M., Gafurov, A., Fohrer, N., & Gupta, H. (2016). Demasking the integrated information of discharge: Advancing sensitivity analysis to consider different hydrological components and their rates of change. *Water Resources Research*, *52*(11), 8724–8743. https://doi.org/10.1002/2016wr018894

Hartmann, A., Barberá, J. A., & Andreo, B. (2017). On the value of water quality observations for karst model parameterization. *Hydrology and Earth System Sciences*, *21*, 5971–5985. https://doi.org/10.5194/hess-21-5971-2017

Her, Y., & Chaubey, I. (2015). Impact of the numbers of observations and calibration parameters on equifinality, model performance, and output and parameter uncertainty. *Hydrological Processes*, *29*(19), 4220–4237. https://doi.org/10.1002/hyp.10487

Hörning, S., & Bárdossy, A. (2018). Phase annealing for the conditional simulation of spatial random fields. *Computers & Geosciences*, *112*, 101–111. https://doi.org/10.1016/j.cageo.2017.12.008

Jefferson, J. L., Gilbert, J. M., Constantine, P. G., & Maxwell, R. M. (2015). Active subspaces for sensitivity analysis and dimension reduction of an integrated hydrologic model. *Computers & Geosciences*, *83*, 127–138. https://doi.org/10.1016/j.cageo.2015.07.001

Jennings, K., & Jones, J. A. (2015). Precipitation-snowmelt timing and snowmelt augmentation of large peak flow events, western Cascades, Oregon. *Water Resources Research*, *51*(9), 7649–7661. https://doi.org/10.1002/2014wr016877

Kelleher, C., McGlynn, B., & Wagener, T. (2017). Characterizing and reducing equifinality by constraining a distributed catchment model with regional signatures, local observations, and process understanding. *Hydrology and Earth System Sciences*, *21*(7), 3325–3352. https://doi.org/10.5194/hess-21-3325-2017

Kollat, J., Reed, P., & Wagener, T. (2012). When are multiobjective calibration trade-offs in hydrologic models meaningful? *Water Resources Research*, *48*(3). https://doi.org/10.1029/2011wr011534

Labat, D. (2005). Recent advances in wavelet analyses: Part 1. A review of concepts. *Journal of Hydrology*, *314*(1–4), 275–288. https://doi.org/10.1016/j.jhydrol.2005.04.003

Labat, D., Ababou, R., & Mangin, A. (2000a). Rainfall–runoff relations for karstic springs. Part I: Convolution and spectral analyses. *Journal of Hydrology*, *238*(3–4), 123–148. https://doi.org/10.1016/s0022-1694(00)00321-8

Labat, D., Ababou, R., & Mangin, A. (2000b). Rainfall–runoff relations for karstic springs. Part II: Continuous wavelet and discrete orthogonal multiresolution analyses. *Journal of Hydrology*, *238*(3–4), 149–178. https://doi.org/10.1016/s0022-1694(00)00322-x

Larocque, M., Mangin, A., Razack, M., & Banton, O. (1998). Contribution of correlation and spectral analyses to the regional study of a large karst aquifer (Charente, France). *Journal of Hydrology*, *205*(3–4), 217–231. https://doi.org/10.1016/s0022-1694(97)00155-8

Mallat, S. G. (1989). A theory for multiresolution signal decomposition: The wavelet representation. *IEEE Transactions on Pattern Analysis and Machine Intelligence*, *11*(7), 674–693. https://doi.org/10.1109/34.192463

Mangin, A. (1984). Pour une meilleure connaissance des systèmes hydrologiques à partir des analyses corrélatoire et spectrale. *Journal of Hydrology*, *67*(1–4), 25–43. https://doi.org/10.1016/0022-1694(84)90230-0

Marcolini, G., Bellin, A., Disse, M., & Chiogna, G. (2017). Variability in snow depth time series in the Adige catchment. *Journal of Hydrology: Regional Studies*, *13*, 240–254. https://doi.org/10.1016/j.ejrh.2017.08.007

Massei, N., Laignel, B., Deloffre, J., Mesquita, J., Motelay, A., Lafite, R., & Durand, A. (2010). Long-term hydrological changes of the Seine River flow (France) and their relation to the North Atlantic Oscillation over the period 1950–2008. *International Journal of Climatology*, *30*(14), 2146–2154. https://doi.org/10.1002/joc.2022

Massmann, C., Wagener, T., & Holzmann, H. (2014). A new approach to visualizing time-varying sensitivity indices for environmental model diagnostics across evaluation time-scales. *Environmental Modelling & Software*, *51*, 190–194. https://doi.org/10.1016/j.envsoft.2013.09.033

Melsen, L. A., & Guse, B. (2021). Climate change impacts model parameter sensitivity–implications for calibration strategy and model diagnostic evaluation. *Hydrology and Earth System Sciences*, *25*(3), 1307–1332. https://doi.org/10.5194/hess-25-1307-2021

Nalley, D., Adamowski, J., & Khalil, B. (2012). Using discrete wavelet transforms to analyze trends in streamflow and precipitation in Quebec and Ontario (1954–2008). *Journal of Hydrology*, *475*, 204–228. https://doi.org/10.1016/j.jhydrol.2012.09.049

Nalley, D., Adamowski, J., Khalil, B., & Biswas, A. (2016). Inter-annual to inter-decadal streamflow variability in Quebec and Ontario in relation to dominant large-scale climate indices. *Journal of hydrology*, *536*, 426–446. https://doi.org/10.1016/j.jhydrol.2016.02.049

Narany, T. S., Bittner, D., Disse, M., & Chiogna, G. (2019). Spatial and temporal variability in hydrochemistry of a small-scale dolomite karst environment. *Environmental Earth Sciences*, *78*(9), 273. https://doi.org/10.1007/s12665-019-8276-2

Nash, J. E., & Sutcliffe, J. V. (1970). River flow forecasting through conceptual models Part I—A discussion of principles. *Journal of Hydrology*, *10*(3), 282–290. https://doi.org/10.1016/0022-1694(70)90255-6

Nowak, K. C., Rajagopalan, B., & Zagona, E. (2011). Wavelet auto-regressive method (warm) for multi-site streamflow simulation of data with non-stationary spectra. *Journal of Hydrology*, *410*(1–2), 1–12. https://doi.org/10.1016/j.jhydrol.2011.08.051

Pérez Ciria, T., & Chiogna, G. (2020). Intra-catchment comparison and classification of long-term streamflow variability in the alps using wavelet analysis. *Journal of Hydrology*, *587*, 124927. https://doi.org/10.1016/j.jhydrol.2020.124927

Pérez Ciria, T., Labat, D., & Chiogna, G. (2019). Detection and interpretation of recent and historical streamflow alterations caused by river damming and hydropower production in the Adige and inn river basins using continuous, discrete and multiresolution wavelet analysis. *Journal of Hydrology*, *578*, 124021. https://doi.org/10.1016/j.jhydrol.2019.124021

Pfannerstill, M., Guse, B., Reusser, D., & Fohrer, N. (2015). Process verification of a hydrological model using a temporal parameter sensitivity analysis. *Hydrology and Earth System Sciences*, *19*(10), 4365–4376. https://doi.org/10.5194/hess-19-4365-2015

Pianosi, F., Beven, K., Freer, J., Hall, J. W., Rougier, J., Stephenson, D. B., & Wagener, T. (2016). Sensitivity analysis of environmental models: A systematic review with practical workflow. *Environmental Modelling & Software*, *79*, 214–232. https://doi.org/10.1016/j.envsoft.2016.02.008

Rathinasamy, M., Khosa, R., Adamowski, J., Ch, S., Partheepan, G., Anand, J., & Narsimlu, B. (2014). Wavelet-based multiscale performance analysis: An approach to assess and improve hydrological models. *Water Resources Research*, *50*(12), 9721–9737. https://doi.org/10.1002/2013wr014650

Razavi, S., & Gupta, H. V. (2015). What do we mean by sensitivity analysis? The need for comprehensive characterization of "global" sensitivity in earth and environmental systems models. *Water Resources Research*, *51*(5), 3070–3092. https://doi.org/10.1002/2014wr016527

Reinecke, R., Foglia, L., Mehl, S., Herman, J. D., Wachholz, A., Trautmann, T., & Döll, P. (2019). Spatially distributed sensitivity of simulated global groundwater heads and flows to hydraulic conductivity, groundwater recharge, and surface water body parameterization. *Hydrology & Earth System Sciences*, *23*(11). https://doi.org/10.5194/hess-23-4561-2019

Rossetto, R., De Filippis, G., Borsi, I., Foglia, L., Cannata, M., Criollo, R., & Vázquez-Suñé, E. (2018). Integrating free and open source tools and distributed modelling codes in GIS environment for data-based groundwater management. *Environmental Modelling & Software*, *107*, 210–230. https://doi.org/10.1016/j.envsoft.2018.06.007

Saltelli, A., Aleksankina, K., Becker, W., Fennell, P., Ferretti, F., Holst, N., et al. (2019). Why so many published sensitivity analyses are false: A systematic review of sensitivity analysis practices. *Environmental Modelling & Software*, *114*, 29–39. https://doi.org/10.1016/j.envsoft.2019.01.012

Saltelli, A., Ratto, M., Andres, T., Campolongo, F., Cariboni, J., Gatelli, D., et al. (2008). *Global sensitivity analysis: The primer*. John Wiley & Sons.

Sang, Y.-F., Wang, Z., & Liu, C. (2013). Discrete wavelet-based trend identification in hydrologic time series. *Hydrological Processes*, *27*(14), 2021–2031. https://doi.org/10.1002/hyp.9356

Schaefli, B., Maraun, D., & Holschneider, M. (2007). What drives high flow events in the Swiss Alps? Recent developments in wavelet spectral analysis and their application to hydrology. *Advances in Water Resources*, *30*(12), 2511–2525. https://doi.org/10.1016/j.advwatres.2007.06.004

Schaefli, B., & Zehe, E. (2009). Hydrological model performance and parameter estimation in the wavelet-domain. *Hydrology and Earth System Sciences*, *13*(10), 1921–1936. https://doi.org/10.5194/hess-13-1921-2009

Schwemmle, R., Demand, D., & Weiler, M. (2021). Diagnostic efficiency–specific evaluation of model performance. *Hydrology and Earth System Sciences*, *25*(4), 2187–2198. https://doi.org/10.5194/hess-25-2187-2021

Shannon, C. E. (1948). A mathematical theory of communication. *Bell system technical journal*, *27*(3), 379–423. https://doi.org/10.1002/j.1538-7305.1948.tb01338.x

Smith, R. C. (2013). Uncertainty quantification: Theory, implementation, and applications (Vol. 12). SIAM.

Song, X., Zhang, J., Zhan, C., Xuan, Y., Ye, M., & Xu, C. (2015). Global sensitivity analysis in hydrological modeling: Review of concepts, methods, theoretical framework, and applications. *Journal of Hydrology*, *523*, 739–757. https://doi.org/10.1016/j.jhydrol.2015.02.013

Tang, Y., Reed, P., Wagener, T., & van Werkhoven, K. (2007). Comparing sensitivity analysis methods to advance lumped watershed model identification and evaluation. *Hydrology and Earth System Sciences*, *11*(2), 793–817. https://doi.org/10.5194/hess-11-793-2007

Teixeira Parente, M., Bittner, D., Mattis, S. A., Chiogna, G., & Wohlmuth, B. (2019). Bayesian calibration and sensitivity analysis for a karst aquifer model using active subspaces. *Water Resources Research*, *55*(8), 7086–7107.

Teixeira Parente, M., Mattis, S., Gupta, S., Deusner, C., & Wohlmuth, B. (2019). Efficient parameter estimation for a methane hydrate model with active subspaces. *Computational Geosciences*, *23*(2), 355–372. https://doi.org/10.1007/s10596-018-9769-x

Torrence, C., & Compo, G. P. (1998). A practical guide to wavelet analysis. *Bulletin of the American Meteorological Society*, *79*(1), 61–78. https://doi.org/10.1175/1520-0477(1998)079<0061:apgtwa>2.0.co;2

Tuo, Y., Marcolini, G., Disse, M., & Chiogna, G. (2018). A multi-objective approach to improve swat model calibration in alpine catchments. *Journal of Hydrology*, *559*, 347–360. https://doi.org/10.1016/j.jhydrol.2018.02.055

Vrugt, J. A., Gupta, H. V., Bastidas, L. A., Bouten, W., & Sorooshian, S. (2003). Effective and efficient algorithm for multiobjective optimization of hydrologic models. *Water Resources Research*, *39*(8). https://doi.org/10.1029/2002wr001746

Wagener, T., & Montanari, A. (2011). Convergence of approaches toward reducing uncertainty in predictions in ungauged basins. *Water Resources Research*, *47*(6). https://doi.org/10.1029/2010wr009469

Wagener, T., & Pianosi, F. (2019). What has Global Sensitivity Analysis ever done for us? A systematic review to support scientific advancement and to inform policy-making in Earth system modelling. *Earth-Science Reviews*, *194*, 1–18. https://doi.org/10.1016/j.earscirev.2019.04.006

Walnut, D. F. (2013). *An introduction to wavelet analysis*. Springer Science & Business Media.

Werkhoven, K., Wagener, T., Reed, P., & Tang, Y. (2008). Characterization of watershed model behavior across a hydroclimatic gradient. *Water Resources Research*, *44*. https://doi.org/10.1029/2007wr006271

Yang, C., Yu, Z., Hao, Z., Zhang, J., & Zhu, J. (2012). Impact of climate change on flood and drought events in Huaihe River Basin, China. *Hydrology Research*, *43*(1–2), 14–22. https://doi.org/10.2166/nh.2011.112

Zolezzi, G., Bellin, A., Bruno, M., Maiolini, B., & Siviglia, A. (2009). Assessing hydrological alterations at multiple temporal scales: Adige River, Italy. *Water Resources Research*, *45*(12), W12421. https://doi.org/10.1029/2008wr007266

References From the Supporting Information

DVWK. (1996). *Ermittlung der Verdunstung von Land- und Wasserflächen*. DVWK-Merkblatt, 238/1996.

Martinec, J. (1960). The degree-day factor for snowmelt runoff forecasting. *IUGG General Assembly of Helsinki, IAHS Commission of Surface Waters*, *51*, 468–477.

Ryan, Ø., Ryan, & Peters (2019). *Linear algebra, signal processing, and wavelets–A unified approach*. Springer.

Teixeira Parente, M., Bittner, D., Mattis, S. A., Chiogna, G., & Wohlmuth, B. (2019). Bayesian calibration and sensitivity analysis for a karst aquifer model using active subspaces. *Water Resources Research*, *55*(8), 7086–7107.

Thornthwaite, C. W. (1948). An approach toward a rational classification of climate. *Geographical Review*, *38*(1), 55–94.

Vannucci, M., & Corradi, F. (1999). Covariance structure of wavelet coefficients: Theory and models in a Bayesian perspective. *Journal of the Royal Statistical Society: Series B*, *61*(4), 971–986.

Walnut, D. F. (2013). *An introduction to wavelet analysis*. Springer Science & Business Media.